Reflective Conditions for Radiative Transfer in Integral Form with Compressed H-Matrices

Olivier Pironneau, Pierre-Henri Tournier

Reflective Conditions for Radiative Transfer in Integral Form with Compressed H-Matrices

Olivier Pironneau and Pierre-Henri Tournier

March 6, 2023

Abstract

In a recent article the authors showed that the radiative Transfer equations with multiple frequencies and scattering can be formulated as a nonlinear integral system. In this article, the formulation is extended to handle reflective boundary conditions. The fixed point method to solve the system is shown to be a monotone. The discretization is done with a P^1 Finite Element Method. The convolution integrals are precomputed at every vertex of the mesh and stored in $2K$ compressed hierarchical matrices, using Partially Pivoted Adaptive Cross-Approximation, where K is the number of different values of absorption. Then the fixed point iterations involve only matrix vector product. The method is $O(N\sqrt[3]{N}\ln N)$, with respect to the number of vertices, when everything is smooth. A numerical implementation is proposed and tested on a simple example. As there are some analogies with ray tracing the programming is complex.

Keywords MSC classification 85A25, 37N30, 31A10, 35Q30, 68P30, 74S05, Radiative Transfer, Reflective boundaries, Integral equation, H-Matrix , Finite Element Methods.

Introduction

The Radiative Transport Equations (RTE) describe the behavior of electromagnetic radiation in a domain Ω as it interacts with matter [13]. It is used to model a wide range of physical phenomena, including the propagation of light through plasma, tomography [17], atmospheric media [12], etc.
The RTE is derived from the basic principles of quantum and statistical mechanics; it is a partial differential equation (PDE) that describes the distribution of radiation intensity in space, time and frequencies, coupled with a budget balance equation (BBE) for the electronic temperature. The PDE takes into

account both absorption and scattering of radiation by matter, as well as emission of radiation by sources, which, in the present case, will be restricted to the boundaries of the emitting material.
In [6],[7] the authors have shown that the PDE can be converted into an integral equation for the total radiation at each point in the domain and that the coupling with the BBE can be handled by fixed point iterations. The method leads also to a general proof of existence, uniqueness and regularity of the solution. The difference with earlier studies such as [4] is in the coupling with the equation for the temperature, BBE or even the full temperature PDE.
In [5] the authors have presented an implementation of the method using H-Matrix compression, a crucial ingredient which makes the evaluation of the integrals $O(N\sqrt[3]{N}\ln N)$ with respect to the number of vertices N in the 3D mesh which discretizes the domain Ω; $N \ln N$ is the complexity of the H-Matrix part but each element of the matrix requires an integral along a line in the domain. Compared with a brute force solution of the equations as in [10], the integral method has still a usable computing time for problems with frequency dependent physical parameters. However it did not handle reflective boundary conditions [16].

H-Matrix compression [8], [1],[3], is a mathematical technique used to efficiently represent and manipulate large matrices that arise in a variety of applications. The technique uses a hierarchical structured representation of the matrices which allows a fast and accurate numerical computations when the integrals have a convolution type integrand which decays with the distance.
H-Matrix compression works by partitioning a large matrix into smaller submatrices, and then approximate these submatrices by hierarchical low-rank approximations. The resulting representation allows for efficient matrix-vector multiplication, among other operations of linear algebra. The technique is particularly important and popular for computational electromagnetics in integral form such as boundary element methods.
With the *Partially Pivoted Adaptive Cross-Approximation* (ACA) [3] only the needed coefficients of the matrices are computed. However the theory requires geometrical smoothness [2].

We have extended the implementation done in [5] using `FreeFEM` [9] and `htool`[1]; `htools` is a C++ toolbox for boundary element methods with electromagnetism in sight. `FreeFEM` is a popular open-source software package used for solving PDE systems with the finite element method (FEM).
`FreeFEM` provides a wide range of pre-built FEM, as well as tools for mesh generation. It has a dedicated high level programming language that allows users to meet their specific needs. `FreeFEM` also supports parallel computing with `mpi`.
One of the main advantages of `FreeFEM` for the present study is its ability to handle complex geometries and boundary condition, especially because of its powerful interpolations from volume to surface meshes.

[1] https://github.com/htool-ddm/htool

Adding reflective conditions (RC) to the `FreeFEM` code presented in [5] turned out to require solving the following difficulties:

- Integrate the RC into the integral formulation of the problem
- Show that the fixed point iterations are still monotone.
- Find a formulation compatible with the use of H-Matrices
- Implement the method in the `FreeFEM` code.

This paper presents the solutions found to resolve these 4 difficulties. It ends with a numerical test proposed in [11].

1 The Radiative Transfer Equations

The problem is formulated in a domain $\Omega \subset \mathbb{R}^3$ with boundary Γ. The unit sphere in $\mathbb{R}^3$ is called $\mathbb{S}^2$. One must find the radiation (called light from now on) intensity $I_\nu(\mathbf{x},\boldsymbol{\omega})$ at all points $\mathbf{x} \in \Omega$, for all directions all $\boldsymbol{\omega} \in \mathbb{S}^2$ and all frequencies $\nu \in \mathbb{R}_+$, satisfying:

$$\boldsymbol{\omega}\cdot\nabla I_\nu + \kappa_\nu I_\nu = \kappa_\nu(1-a_\nu)B_\nu(T) + \kappa_\nu a_\nu J_\nu\,, \quad J_\nu := \tfrac{1}{4\pi}\int_{\mathbb{S}^2} I_\nu \mathrm{d}\boldsymbol{\omega}\,, \tag{1}$$

$$\int_0^\infty \kappa_\nu(1-a_\nu)(J_\nu - B_\nu(T))\mathrm{d}\nu = 0\,, \tag{2}$$

$$I_\nu(\mathbf{x},\boldsymbol{\omega}) = R_\nu(\mathbf{x},\boldsymbol{\omega})I_\nu(\mathbf{x},\boldsymbol{\omega}-2(\mathbf{n}\cdot\boldsymbol{\omega})\mathbf{n}) + Q_\nu(\mathbf{x},\boldsymbol{\omega}),$$
$$\text{on } \Sigma := \{(\mathbf{x},\boldsymbol{\omega}) \in \Gamma\times\mathbb{S}^2 \ : \ \boldsymbol{\omega}\cdot\mathbf{n}(\mathbf{x}) < 0\}, \tag{3}$$

where $B_\nu(T) = \frac{\nu^3}{\mathrm{e}^{\frac{\nu}{T}}-1}$ is the (rescaled) Planck function. In the RC (3), R_ν is the portion of light which is reflected and Q_ν is the light source; $\mathbf{n}(\mathbf{x})$ is the outer normal of Γ at $\mathbf{x}$. κ_ν and a_ν are the absorption and scattering coefficients; in general they depend on ν and $\mathbf{x}$.

Example 1 *If an object $\mathcal{O}$ inside a box $\mathcal{B}$ radiates because it is at temperature T_0, then, $\Omega = \mathcal{O}\backslash\mathcal{B}$, $Q_\nu = Q^0[\boldsymbol{\omega}\cdot\mathbf{n}]_- B_\nu(T_0)$ on $\mathcal{O}$ and zero elsewhere and $\Sigma \subset \partial\mathcal{B}\times\mathbb{S}^2$.*

1.1 An Integral Formulation

For clarity we drop the subscript ν on κ, a and I. Assume that Ω is bounded and convex (see remark 1). Let

$$S_\nu(\mathbf{x}) = \kappa(1-a)B_\nu(T) + \kappa a J_\nu, \tag{4}$$

For a given $\mathbf{x}$ and $\boldsymbol{\omega}$, let $\tau_{\mathbf{x},\boldsymbol{\omega}}$ be such that $(\mathbf{x}_\Sigma(\mathbf{x},\boldsymbol{\omega}) := \mathbf{x} - \tau_{\mathbf{x},\boldsymbol{\omega}}\boldsymbol{\omega},\boldsymbol{\omega}) \in \Sigma$; the method of characteristics tells us that

$$I(\mathbf{x},\boldsymbol{\omega}) = I(\mathbf{x}_\Sigma(\mathbf{x},\boldsymbol{\omega}),\boldsymbol{\omega})\mathrm{e}^{-\int_0^{\tau_{\mathbf{x},\boldsymbol{\omega}}}\kappa(\mathbf{x}-\boldsymbol{\omega}s)\mathrm{d}s} + \int_0^{\tau_{\mathbf{x},\boldsymbol{\omega}}} \mathrm{e}^{-\int_0^s \kappa(\mathbf{x}-\boldsymbol{\omega}s')\mathrm{d}s'} S_\nu(\mathbf{x}-\boldsymbol{\omega}s)\mathrm{d}s. \tag{5}$$

Notice that $\tau_{\mathbf{x},\boldsymbol{\omega}} = |\mathbf{x}_\Sigma - \mathbf{x}|$ (see Figure 1), therefore, let

$$\begin{aligned} J_\nu(\mathbf{x}) &:= \tfrac{1}{4\pi}\int_{\mathbb{S}^2} I(\mathbf{x},\boldsymbol{\omega})\mathrm{d}\omega = S^E_\nu(\mathbf{x}) + \mathcal{J}[S_\nu](\mathbf{x}) \quad \text{with} \\ S^E_\nu(\mathbf{x}) &:= \tfrac{1}{4\pi}\int_{\mathbb{S}^2} I(\mathbf{x}_\Sigma(\mathbf{x},\boldsymbol{\omega}),\boldsymbol{\omega})\mathrm{e}^{-\int_0^{\tau_{\mathbf{x},\boldsymbol{\omega}}}\kappa(\mathbf{x}-\boldsymbol{\omega}s)\mathrm{d}s}\mathrm{d}\omega, \\ \mathcal{J}[S](\mathbf{x}) &:= \tfrac{1}{4\pi}\int_{\mathbb{S}^2}\int_0^{\tau_{\mathbf{x},\boldsymbol{\omega}}} \mathrm{e}^{-\int_0^s \kappa(\mathbf{x}-\boldsymbol{\omega}s')\mathrm{d}s'} S(\mathbf{x}-\boldsymbol{\omega}s)\mathrm{d}s\mathrm{d}\omega \\ &= \tfrac{1}{4\pi}\int_\Omega S(\mathbf{y})\frac{\mathrm{e}^{-\int_{[\mathbf{x},\mathbf{y}]}\kappa}}{|\mathbf{y}-\mathbf{x}|^2}\mathrm{d}\mathbf{y}. \end{aligned} \tag{6}$$

where, $\boldsymbol{\omega}'(\boldsymbol{\omega}) := \boldsymbol{\omega} - 2(\mathbf{n}\cdot\boldsymbol{\omega})\mathbf{n}$ and $\int_{[\mathbf{x},\mathbf{y}]} f := |\mathbf{y}-\mathbf{x}|\int_0^1 f(s\mathbf{y}+(1-s)\mathbf{x})\mathrm{d}s$. To justify the last formula we refer to the following lemma with $\Psi(\mathbf{x},\mathbf{y}) = S(\mathbf{y})\mathrm{e}^{-\int_{[\mathbf{x},\mathbf{y}]}\kappa}$. Again, for clarity, we drop the first argument $\mathbf{x}$.

Lemma 1 *Let Ω be a convex bounded open set of $\mathbb{R}^3$; let Γ be its boundary. Let $\Psi : \Omega \mapsto \mathbb{R}$ be continuous. Let $\tau_{\mathbf{x},\boldsymbol{\omega}} \geq 0$ be such that $\mathbf{x} - \tau_{\mathbf{x},\boldsymbol{\omega}}\boldsymbol{\omega} \in \Gamma$, $\mathbf{x} \in \Omega$. Then*

$$\int_{\mathbb{S}^2}\int_0^{\tau_{\mathbf{x},\boldsymbol{\omega}}} \Psi(\mathbf{x}-\boldsymbol{\omega}s)\mathrm{d}s\mathrm{d}\omega = \int_\Omega \frac{\Psi(\mathbf{y})}{|\mathbf{y}-\mathbf{x}|^2}\mathrm{d}\mathbf{y}.$$

Proof: Denote $\tilde{\Psi}$ the extension of Ψ by zero outside Ω. Let $\boldsymbol{\omega} = (\cos\theta\sin\varphi, \sin\theta\sin\varphi, \cos\varphi)^T$, $\theta \in (0, 2\pi)$, $\varphi \in (-\frac{\pi}{2}, \frac{\pi}{2})$. Consider a partition of the semi infinite line starting at $\mathbf{x}$ in direction $-\boldsymbol{\omega}$ into segments of size δs and denote $\mathbf{x}_n = \mathbf{x} - n\delta s\boldsymbol{\omega}$. Then

$$\begin{aligned} \int_{\mathbb{S}^2}\int_0^{\tau_{\mathbf{x},\boldsymbol{\omega}}} \tilde{\Psi}(\mathbf{x}-\boldsymbol{\omega}s)\mathrm{d}s\mathrm{d}\omega &= \lim_{\delta s\to 0}\sum_{n>0}\delta s\int_0^{2\pi}\int_{-\frac{\pi}{2}}^{\frac{\pi}{2}} \tilde{\Psi}(\mathbf{x}_n)\cos\varphi\mathrm{d}\varphi\mathrm{d}\theta \\ &= \lim_{\delta s\to 0}\sum_{n>0}\int_0^{2\pi}\int_{-\frac{\pi}{2}}^{\frac{\pi}{2}} \frac{\tilde{\Psi}(\mathbf{x}_n)}{|\mathbf{x}-\mathbf{x}_n|^2}|\mathbf{x}-\mathbf{x}_n|^2|\mathbf{x}_{n+1}-\mathbf{x}_n|\cos\varphi\mathrm{d}\varphi\mathrm{d}\theta \end{aligned} \tag{7}$$

We note that $|\mathbf{x}-\mathbf{x}_n|^2|\mathbf{x}_{n+1}-\mathbf{x}_n|\cos\varphi\mathrm{d}\theta\mathrm{d}\varphi$ is the elementary volume in the sector $\mathrm{d}\theta\mathrm{d}\varphi$ between the spheres centered at $\mathbf{x}$ and of radii $|\mathbf{x}-\mathbf{x}_n|$ and $|\mathbf{x}-\mathbf{x}_{n+1}|$. Therefore the right handside is an integral in $\mathbf{x}' \in \mathbb{R}^3$ of $\frac{\tilde{\Psi}(\mathbf{y})}{|\mathbf{x}-\mathbf{y}|^2}|\mathbf{x}-\mathbf{x}_n|^2$. □

Remark 1 *When Ω is not convex, on may apply the lemma to its convex closure $\bar{\Omega}$ with κ extended to $+\infty$ in $\bar{\Omega}\backslash\Omega$.*

Remark 2 *When $R_\nu \equiv 0$, S^E is known. As (2) defines a map $\mathcal{T} : J \mapsto T$,*

$$T(\mathbf{x}) = \mathcal{T}[J_\nu](\mathbf{x}), \quad \forall \mathbf{x} \in \Omega,$$

then, (4), (6) is a nonlinear integral formulation for J:

$$J_\nu(\mathbf{x}) = S^E_\nu(\mathbf{x}) + \mathcal{J}[\kappa(1-a)B_\nu(\mathcal{T}[J_\nu]) + \kappa a J_\nu](\mathbf{x}), \quad \forall \mathbf{x} \in \Omega. \tag{8}$$

The following fixed point method was shown in [6] to be monotone and convergent:

$$J_\nu^{k+1}(\mathbf{x}) = S_\nu^E(\mathbf{x}) + \mathcal{J}[\kappa(1-a)B_\nu(\mathcal{T}[J_\nu^k](\mathbf{x})) + \kappa a J_\nu^k](\mathbf{x}), \quad k = 0, 1, \ldots \tag{9}$$

Let us extend these properties to the RTE with RCs.
For clarity let $\mathbf{x}_\Sigma$ be short for $\mathbf{x}_\Sigma(\mathbf{x}, \boldsymbol{\omega})$ and let $\boldsymbol{\omega}'$ be

$$\boldsymbol{\omega}'(\boldsymbol{\omega}) = \boldsymbol{\omega} - 2\boldsymbol{\omega} \cdot \mathbf{n}(\mathbf{x}')\, \mathbf{n}(\mathbf{x}'), \qquad \text{with } \boldsymbol{\omega} = \frac{\mathbf{x} - \mathbf{x}'}{|\mathbf{x} - \mathbf{x}'|}.$$

Let us insert (5) and (3) in (6). Then,

$$\begin{aligned}
&S_\nu^E(\mathbf{x}) = S_{\nu,1}^E + S_{\nu,2}^E + S_{\nu,3}^E \text{ with} \\
&S_{\nu,1}^E(\mathbf{x}) := \tfrac{1}{4\pi} \int_{\mathbb{S}^2} Q_\nu(\mathbf{x}_\Sigma, \boldsymbol{\omega}) \mathrm{e}^{-\int_0^{\tau_{\mathbf{x},\boldsymbol{\omega}}} \kappa(\mathbf{x}-\boldsymbol{\omega}s)\mathrm{d}s} \mathrm{d}\omega, \\
&S_{\nu,2}^E(\mathbf{x}) := \tfrac{1}{4\pi} \int_{\mathbb{S}^2} R_\nu(\mathbf{x}_\Sigma, \boldsymbol{\omega}) Q_\nu(\mathbf{x}_\Sigma(\mathbf{x}_\Sigma, \boldsymbol{\omega}'), \boldsymbol{\omega}') \Big[\mathrm{e}^{-\int_0^{\tau_{\mathbf{x}_\Sigma,\boldsymbol{\omega}'}} \kappa(\mathbf{x}_\Sigma - \boldsymbol{\omega}' s)\mathrm{d}s} \\
&\qquad\qquad \mathrm{e}^{-\int_0^{\tau_{\mathbf{x},\boldsymbol{\omega}}} \kappa(\mathbf{x}-\boldsymbol{\omega}s)\mathrm{d}s} \Big] \mathrm{d}\omega, \\
&S_{\nu,3}^E(\mathbf{x}) := \tfrac{1}{4\pi} \int_{\mathbb{S}^2} \Big[R_\nu(\mathbf{x}_\Sigma, \boldsymbol{\omega}) \mathrm{e}^{-\int_0^{\tau_{\mathbf{x},\boldsymbol{\omega}}} \kappa(\mathbf{x}-\boldsymbol{\omega}s')\mathrm{d}s'} \\
&\qquad\qquad \int_0^{\tau_{\mathbf{x}_\Sigma,\boldsymbol{\omega}'}} \mathrm{e}^{-\int_0^s \kappa(\mathbf{x}_\Sigma - \boldsymbol{\omega}' s')\mathrm{d}s'} S_\nu(\mathbf{x}_\Sigma - \boldsymbol{\omega}' s)\mathrm{d}s \Big] \mathrm{d}\omega.
\end{aligned}$$

Hypothesis 1 *Let us rule out multiple reflections and focal points*

1. *If* $R_\nu(\mathbf{x}_\Sigma(\mathbf{x}, \boldsymbol{\omega}), \boldsymbol{\omega}) > 0$, *then* $R_\nu(\mathbf{x}_\Sigma(\mathbf{x}_\Sigma(\mathbf{x}, \boldsymbol{\omega}), \boldsymbol{\omega}'), \boldsymbol{\omega}) = 0$.
2. *Given* $\mathbf{x}$ *and* $\mathbf{y}$, *there is only a finite number* N *of* $\mathbf{x}'_n \in \Gamma$ *such that* $[\mathbf{x}'_n, \mathbf{y}]$ *is the reflected ray of* $[\mathbf{x}, \mathbf{x}'_n]$. *Note that* $\mathbf{x}'_n$ *depends on* $\mathbf{x}$ *and* $\mathbf{y}$.

Proposition 1 *Under Hypothesis 1*

$$S_{\nu,3}^E(\mathbf{x}) := \sum_{n=1}^{M} \tfrac{1}{4\pi} \int_\Omega R_\nu(\mathbf{x}'_n, \tfrac{\mathbf{x}-\mathbf{x}'_n}{|\mathbf{x}-\mathbf{x}'_n|}) \frac{\mathrm{e}^{-\int_{[\mathbf{x},\mathbf{x}'_n]\cup[\mathbf{x}'_n,\mathbf{y}]} \kappa}}{(|\mathbf{x}-\mathbf{x}'_n| + |\mathbf{x}'_n - \mathbf{y}|)^2} S(\mathbf{y}) \mathrm{d}\mathbf{y}$$

Proof Let $\mathbf{x}(s) := \mathbf{x}_\Sigma - \omega' s$. By Lemma 1, (7) can be written as

$$\begin{aligned}
&\int_{\mathbb{S}^2} \int_0^{\tau_{\mathbf{x}_\Sigma,\boldsymbol{\omega}'}} \Big[R_\nu(\mathbf{x}_\Sigma, \boldsymbol{\omega}) \mathrm{e}^{-\int_{[\mathbf{x},\mathbf{x}_\Sigma]\cup[\mathbf{x}_\Sigma,\mathbf{x}(s)]} \kappa} S(\mathbf{x}(s))\mathrm{d}s \Big] \mathrm{d}\omega \\
&\qquad = \int_\Omega R_\nu(\mathbf{x}_\Sigma, \boldsymbol{\omega}) S(\mathbf{y}) \frac{\mathrm{e}^{-\int_{[\mathbf{x},\mathbf{x}_\Sigma]\cup[\mathbf{x}_\Sigma,\mathbf{y}]} \kappa}}{(|\mathbf{x}-\mathbf{x}_\Sigma| + |\mathbf{x}_\Sigma - \mathbf{y}|)^2} \mathrm{d}\mathbf{y},
\end{aligned}$$

provided that $[\mathbf{x}_\Sigma, \mathbf{y}]$ is reflected from $[\mathbf{x}, \mathbf{x}_\Sigma]$. Now, by hypothesis, if $\mathbf{x}$ and $\mathbf{y}$ are given in Ω there are only a finite number of $\mathbf{x}_\Sigma \in \Gamma$ for which $[\mathbf{x}_\Sigma, \mathbf{y}]$ is reflected from $[\mathbf{x}, \mathbf{x}_\Sigma]$, (see Figure 1). □

Proposition 2 *Let Hypothesis 1 hold. Then the source terms from the boundaries are*

$$S^E_{\nu,1}(\mathbf{x}) = \tfrac{1}{4\pi}\int_\Gamma Q_\nu(\mathbf{y}, \tfrac{\mathbf{y}-\mathbf{x}}{|\mathbf{y}-\mathbf{x}|})\frac{[(\mathbf{y}-\mathbf{x})\cdot\mathbf{n}(\mathbf{y})]_-}{|\mathbf{y}-\mathbf{x}|^3}\mathrm{e}^{-\int_{[\mathbf{x},\mathbf{y}]}\kappa}\mathrm{d}\Gamma(\mathbf{y}), \tag{10}$$

$$S^E_{\nu,2}(\mathbf{x}) = \sum_{n=1}^{M}\tfrac{1}{4\pi}\int_\Gamma R_\nu(\mathbf{x}'_n, \tfrac{\mathbf{x}-\mathbf{x}'}{|\mathbf{x}-\mathbf{x}'|})Q_\nu(\mathbf{y}, \tfrac{\mathbf{x}'_n-\mathbf{y}}{|\mathbf{x}'_n-\mathbf{y}|}) \frac{[(\mathbf{x}'_n-\mathbf{y})\cdot\mathbf{n}(\mathbf{y})]_-\mathrm{e}^{-\int_{[\mathbf{x},\mathbf{x}'_n]\cup[\mathbf{x}'_n,\mathbf{y}]}\kappa}}{|\mathbf{x}'_n-\mathbf{y}|\,(|\mathbf{x}-\mathbf{x}'_n|+|\mathbf{x}'_n-\mathbf{y}|)^2}\mathrm{d}\Gamma(\mathbf{y}). \tag{11}$$

Recall that $\mathbf{x}'_n$ *depends* $\mathbf{y}$.

Proof : Recall that a solid angle integral at $\mathbf{x}$ of a surface Σ is

$$\int_{\mathbb{S}^2} f(\mathbf{x},\mathbf{x}')\mathrm{d}\boldsymbol{\omega}(\mathbf{x}') = \int_\Sigma f(\mathbf{x},\mathbf{x}')\frac{[(\mathbf{x}-\mathbf{x}')\cdot\mathbf{n}(\mathbf{x}')]_-}{|\mathbf{x}-\mathbf{x}'|}\frac{\mathrm{d}\Sigma(\mathbf{x}')}{|\mathbf{x}-\mathbf{x}'|^2},$$

Hence from the definition of $S^E_{\nu,2}$ above we see that (10) holds.
To prove (11) we start from the definition of $S^E_{\nu,2}$ above. For clarity let us assume that Q_ν and R_ν do not depend on $\boldsymbol{\omega}$.
Observe that if a ray from $\mathbf{x}$ in the direction $-\boldsymbol{\omega}$ does not hit, after reflection at $\mathbf{x}'$ on some Γ_R, a boundary Γ_Q at $\mathbf{y}$ where $Q_\nu(\mathbf{y})$ is non zero then that $\boldsymbol{\omega}$ does not contribute to $S^E_{\nu,2}$. So we can use the solid angle of Γ_Q. However the solid angle is not seen from $\mathbf{x}$ but from $\bar{\mathbf{x}}$, the symmetric of $\mathbf{x}$ with respect to the tangent plane of Γ_R at $\mathbf{x}'$. As the distance from $\bar{\mathbf{x}}$ to $\mathbf{y}$ is also $|\mathbf{x}-\mathbf{x}'|+|\mathbf{x}'-\mathbf{y}|$, we obtain (11). □

Corollary 1

$$J_\nu(\mathbf{x}) = \bar{S}^E_\nu(\mathbf{x}) + \bar{\mathcal{J}}[S_\nu](\mathbf{x}), \tag{12}$$

with $\bar{S}^E_\nu(\mathbf{x}) := S^E_{\nu,1}(\mathbf{x}) + S^E_{\nu,2}(\mathbf{x})$ *given by Proposition 2 and*

$$\bar{\mathcal{J}}[S](\mathbf{x}) = \tfrac{1}{4\pi}\int_\Omega\left[\frac{\mathrm{e}^{-\int_{[\mathbf{x},\mathbf{y}]}\kappa}}{|\mathbf{y}-\mathbf{x}|^2} + \sum_{n=1}^{M}\frac{\mathrm{e}^{-\int_{[\mathbf{x},\mathbf{x}'_n]\cup[\mathbf{x}'_n,\mathbf{y}]}\kappa}}{(|\mathbf{x}-\mathbf{x}'_n|+|\mathbf{x}'_n-\mathbf{y}|)^2}R_\nu(\mathbf{x}'_n, \tfrac{\mathbf{x}-\mathbf{x}'_n}{|\mathbf{x}-\mathbf{x}'_n|})\right]S(\mathbf{y})\mathrm{d}\mathbf{y} \tag{13}$$

1.2 Example

Assume that $\Gamma = \Gamma_Q \cup \Gamma_R$ and $Q_\nu(\mathbf{x},\boldsymbol{\omega}) = [\boldsymbol{\omega}\cdot\mathbf{n}(\mathbf{x})]_-\, Q^0$ with $Q^0 > 0$ on Γ_Q and 0 on Γ_R. Assume $R_\nu(\mathbf{x},\boldsymbol{\omega}) = R^0$ with $R_0 > 0$ on Γ_R and 0 on Γ_Q. Assume that

there is never more than one reflection point on Γ_R, i.e. $N = 1$. Then

$$\bar{S}^E_\nu(\mathbf{x}) = \frac{Q^0}{4\pi}\int_{\Gamma_Q}\left[\left(\frac{[(\mathbf{y}-\mathbf{x})\cdot\mathbf{n}(\mathbf{y})]_-}{|\mathbf{y}-\mathbf{x}|^2}\right)^2 \mathrm{e}^{-\int_{[\mathbf{x},\mathbf{y}]}\kappa} + R^0\frac{([(\mathbf{x}'_1-\mathbf{y})\cdot\mathbf{n}(\mathbf{y})]_-)^2\mathrm{e}^{-\int_{[\mathbf{x},\mathbf{x}'_1]\cup[\mathbf{x}'_1,\mathbf{y}]}\kappa}}{|\mathbf{x}'_1-\mathbf{y}|^2\,(|\mathbf{x}-\mathbf{x}'_1|+|\mathbf{x}'_1-\mathbf{y}|)^2}\right]\mathrm{d}\Gamma(\mathbf{y}),$$

$$\bar{\mathcal{J}}[S](\mathbf{x}) = \tfrac{1}{4\pi}\int_\Omega\left[\frac{\mathrm{e}^{-\int_{[\mathbf{x},\mathbf{y}]}\kappa}}{|\mathbf{y}-\mathbf{x}|^2} + R^0\frac{\mathrm{e}^{-\int_{[\mathbf{x},\mathbf{x}'_1]\cup[\mathbf{x}'_1,\mathbf{y}]}\kappa}}{(|\mathbf{x}-\mathbf{x}'_1|+|\mathbf{x}'_1-\mathbf{y}|)^2}\right]S(\mathbf{y})\mathrm{d}\mathbf{y}.$$

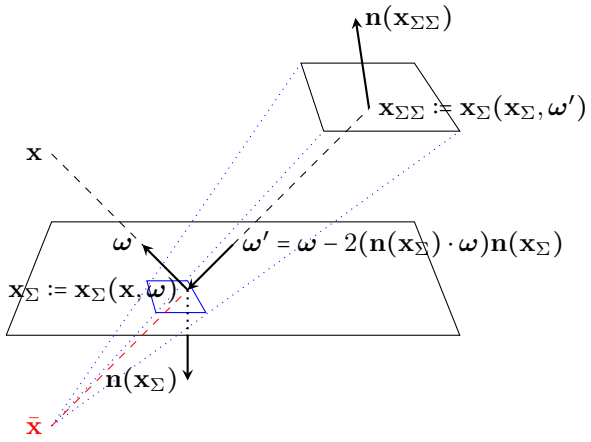

Figure 1: In this configuration the source Γ_Q is the upper square. An RC is imposed on the lower plane Γ_R. S^E_ν has an integral of the solid angle of the upper square seen from $\mathbf{x}$ plus an integral of the solid angle of the upper square seen from $\bar{\mathbf{x}}$, the symmetric of $\mathbf{x}$ with respect to Γ_R.

1.3 Fixed Point Iterations

Consider the fixed point iterations initialized with T^0 and $J^0 = 0$.

Algorithm For $k = 0, 1, \ldots$:

Set $S^k_\nu(\mathbf{x}) = \kappa(1-a)B_\nu(T^k) + \kappa a J^k_\nu$,

Set $J^{k+1}_\nu(\mathbf{x}) = \bar{S}^E_\nu(\mathbf{x}) + \bar{\mathcal{J}}[S^k_\nu](\mathbf{x})$.

Compute T^{k+1} by solving (using Newton algorithm) for each $\mathbf{x} \in \Omega$ (14)

$$\int_0^\infty \kappa_\nu(1-a_\nu)(J^{k+1}_\nu - B_\nu(T^{k+1}))\mathrm{d}\nu = 0.$$

Proposition 3 *Let $\{J_\nu^*, T^*\}$ be the solution. If $T^0(\mathbf{x}) > T^*(\mathbf{x}),\ \forall \mathbf{x} \in \Omega$ then the iterations are monotone decreasing: $T^k(\mathbf{x}) > T^{k+1} > T^*(\mathbf{x}),\ \forall \mathbf{x} \in \Omega$. Conversely if $T^0(\mathbf{x}) < T^*(\mathbf{x}),\ \forall \mathbf{x} \in \Omega$ then the iterations are monotone increasing: $T^k(\mathbf{x}) < T^{k+1} < T^*(\mathbf{x}),\ \forall \mathbf{x} \in \Omega$.*

Proof : Le us prove it for the monote increasing sequence.
By subtracting the definition J_ν^k from that of J_ν^{k+1} and using the linearity of $\bar{\mathcal{J}}$, we obtain

$$J_\nu^{k+1}(\mathbf{x}) - J_\nu^k(\mathbf{x}) = \bar{\mathcal{J}}[S_\nu^k - S_\nu^{k-1}](\mathbf{x}).$$

As $\mathcal{J}$ is a strictly positive operator, if $S_\nu^k > S_\nu^{k-1}$ for all $\mathbf{x}$ then $J_\nu^{k+1}(\mathbf{x}) > J_\nu^k(\mathbf{x})$.
The equation for T^{k+1} is also monotone in the sense that

$$J_\nu^k(\mathbf{x}) > J_\nu^k(\mathbf{x}) \quad \Longrightarrow \quad B_\nu(T^{k+1}) > B_\nu(T^k) \quad \Longrightarrow \quad T^{k+1} > T^k,$$

because B_ν is increasing in T.
Conclusion: if $T^1 > T^0$ and $S^1 > S^0$ then $T^{k+1} > T^k$ for all k. One sure way to impose it is to choose $T^0 = 0$ and $J^0 = 0$.
To prove that $T^k < T^*$ we observe that

$$J_\nu^k(\mathbf{x}) - J_\nu^*(\mathbf{x}) = \bar{\mathcal{J}}[S_\nu^{k-1} - S_\nu^*](\mathbf{x}).$$
$$\text{Hence } S_\nu^{k-1} < S_\nu^* \quad \Longrightarrow \quad J_\nu^k(\mathbf{x}) < J_\nu^*(\mathbf{x}) \quad \Longrightarrow \quad T^k < T^*.$$

□

Remark 3 *Henceforth, convergence and uniqueness can probably be proved as in [7], but there are technical difficulties of functional analysis which may not be appropriately discussed here.*

2 FEM discretization and Compressed H-Matrices

For clarity consider exemple 1.2. As the values of Q^0 and R^0 depend on the boundary name, we write $Q^0(\mathbf{x})$ and $R^0(\mathbf{x})$.
The domain Ω is discretized by a tetraedral mesh; the boundary Γ is discretized by triangular mesh, not necessarily conforming with the volume mesh.
Let $\{\mathbf{x}^j\}_1^N$ be the vertices of the tetraedra of Ω and $\{\tilde{\mathbf{x}}^l\}_1^L$ the vertices of the triangles of Γ .
A continuous P^1 interpolation of J on the tetraedral mesh is:

$J(\mathbf{x}) = \sum_1^N J_j \hat{w}^j(\mathbf{x})$ where $\hat{w}^j$ is the P^1- Finite Element hat function of vertex $\mathbf{x}^j$.

Then

$$S_{\nu,j} := aJ_{\nu,j} + (1-a)B_\nu(T_j), \quad J_{\nu,i} := \bar{S}^E_{\nu,i} + \sum_j G^{ij}_\kappa S_{\nu,j} \qquad \text{where}$$

$$G^{ij}_\kappa = \frac{1}{4\pi}\int_\Omega \left[\kappa \frac{\mathrm{e}^{-\int_{[\mathbf{x}^i-\mathbf{y}]}\kappa}}{|\mathbf{x}^i-\mathbf{y}|^2}\mathrm{d}y + \sum_{n=1}^{M} R^0(\mathbf{x}'_n)\frac{\mathrm{e}^{-\int_{[\mathbf{x}^i,\mathbf{x}'_n]\cup[\mathbf{x}'_n,\mathbf{y}]}\kappa}}{(|\mathbf{x}^i-\mathbf{x}'_n|+|\mathbf{x}'_n-\mathbf{y}|)^2}\right]\hat{w}^j(\mathbf{y})\mathrm{d}\mathbf{y}$$

$$\text{and where } \bar{S}^E_{\nu,i} = \frac{1}{4\pi}\int_\Gamma Q^0(\mathbf{y})\left[\left(\frac{[(\mathbf{x}^i-\mathbf{y})\cdot\mathbf{n}(\mathbf{y})]_-}{|\mathbf{x}^i-\mathbf{y}|^2}\right)^2 \mathrm{e}^{-\int_{[\mathbf{x}^i,\mathbf{y}]}\kappa}\right.$$

$$\left. + \sum_{n=1}^{M} R^0(\mathbf{x}'_n)\frac{([(\mathbf{x}'_n-\mathbf{y})\cdot\mathbf{n}(\mathbf{y})]_-)^2\mathrm{e}^{-\int_{[\mathbf{x}^i,\mathbf{x}'_n]\cup[\mathbf{x}'_n,\mathbf{y}]}\kappa}}{|\mathbf{x}'_n-\mathbf{y}|^2(|\mathbf{x}^i-\mathbf{x}'_n|+|\mathbf{x}'_n-\mathbf{y}|)^2}\right]\mathrm{d}\Gamma(\mathbf{y})$$

The integrals are approximated with quadrature at points $\{\mathbf{x}^j_q\}_1^{M_q}$. The points are inside the elements; consequently $|\mathbf{x}^i-\mathbf{x}^j_q|$ is never zero. A formula of degree 5, with $M_q = 14$, is used when $|\mathbf{x}^i-\mathbf{y}|$ is small and of degree 2, with $M_q = 4$, otherwise; the results do not change when higher degrees are used. Luckily when $\mathbf{x}^i$ is closed to Γ an analytical formula can be used [7].
To compute $\mathbf{x}'_n$ such that $[\mathbf{y},\mathbf{x}'_n]$ is the reflected ray of $[\mathbf{x}'_n,\mathbf{x}^i]$ a loop on all the elements of the reflecting boundaries is necessary. This can be expensive, but in the case of planar reflective boundaries the symmetric point $\bar{\mathbf{x}}^i$ is easy to compute and so is the intersection of $[\bar{\mathbf{x}}^i,\mathbf{y}]$ with the reflective boundary.
Finally, to the vector $\{\bar{S}^E_{\nu,i}\}_{i=1}^N$ we associate a matrix $\{\bar{S}^E_{i,l}\}_{i,l=1}^{N,L}$ by replacing $Q^0(\mathbf{y})$ above by $\tilde{w}^l(\mathbf{y})$. Then:

$$Q^0(\mathbf{y}) = \sum_1^L Q^0_l\tilde{w}^l(\mathbf{y}) \implies \bar{S}^E_{\nu,i} = \sum_1^L \bar{S}^E_{i,l}Q^0_l.$$

2.1 Compression

So, for each ν we have two very large matrices, $\{\bar{G}_{i,j}\}_{i,j=1}^{N,N}$ and $\{\bar{S}^E_{i,l}\}_{i,l=1}^{N,L}$.

Remark 4 *Note that for each value of ν two matrices are needed. However on close inspection it is really two matrices for each value of κ_ν. Very often, less than ten values are sufficient to represent a general κ_ν.*

Both matrices can be compressed as $\mathcal{H}$-matrix [2],[14],[15] (and the references therein) so that the matrix-vector product has complexity $O(N\ln N)$.
The method works best when the kernel in the integrals, decays with the distance between $\mathbf{x}^i$ and $\mathbf{y}$. In both matrices the kernel decays with the square of the distance. The $\mathcal{H}$-matrix approximation views $\mathbf{G}$ as a hierarchical tree of square blocks. The blocks correspond to interactions between clusters of points near $\mathbf{x}^j$ and near $\mathbf{x}^i$. A far-field interaction block can be approximated by a low rank matrix because its singular value decomposition (SVD) has a fast decaying singular value. We use the *Partially Pivoted Adaptive Cross-Approximation* (ACA) [3], to approximate the first terms of the SVD of the blocks, because

only r-rows times r-columns are needed instead of the whole block, where r is the rank of the approximation. The rank is a function of a user defined parameter ϵ connected to the relative Frobenius norm error. Another criteria must be met: if R_1 (resp. R_2) is the radius of a cluster of points centered at $\mathbf{x}_1$ (resp. $\mathbf{x}_2$), then one goes down the hierarchical tree until the corresponding block satisfies $\max(R_1, R_2) < \eta|\mathbf{x}_1 - \mathbf{x}_2|$ where η is a user defined parameter. If the end of the tree is reached, the block is not compacted.
The precision is not guaranteed on account of $[(\mathbf{x}-\mathbf{y})\cdot\mathbf{n}(\mathbf{y})]_-$ if the jump from one triangular face to another is large. A similar singularity caused by normals is analyzed for a double layer potential formulation in [2] (Example 3.38, p148) and a remedy is proposed. To check whether this remedy is needed here we ran two cases, one without compression and one with 97% compression. No difference was observed.

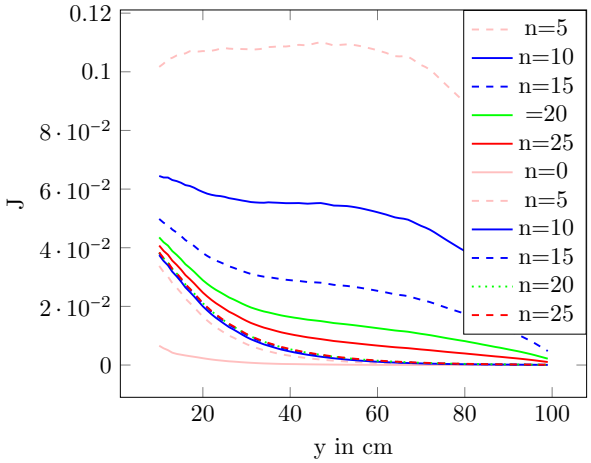

Figure 2: Values of J along the y axis at $x = z = 15$ computed with a RC. Convergence versus iteration number n. When the scaled temperature is initialized to $T^0 = 0.001$ at $n = 0$ the convergence is monotonously increasing. When $T^0 = 0.44$ the convergence is monotonously decreasing.

3 A Test Case

In [11] a semi-analytic solution of the RTE is given for a geometry shown on Figure 3. In this test $a = 0$ and κ is not a function of ν. Hence the grey formulation can be used. Define $\bar{I} = \int_0^\infty I_\nu \mathrm{d}\nu$. By averaging (14) in ν and due to the Stefan-Boltzmann relation, the following holds (for clarity $a_\nu = 0$):

$$\begin{aligned} &\int_0^\infty B_\nu(T)\mathrm{d}\nu = \sigma T^4 \text{ with } \sigma = \frac{\pi^4}{15} \quad \Longrightarrow \\ &\bar{J}^{k+1}(\mathbf{x}) = \bar{S}^E(\mathbf{x}) + \bar{\mathcal{J}}[\kappa\sigma(T^k)^4](\mathbf{x}), \quad \kappa\sigma(T^{k+1})^4 = \kappa\bar{J}^{k+1}. \end{aligned} \tag{15}$$

3.1 The Geometry

The outer container is $D = (0,60) \times (0,100) \times (0,60)$, in cm. A cube $C = [0,10]^3$ radiates with intensity $Q^0 = 0.1$. A rectangular cylinder prolonging the radiating cube $(0,10) \times (10,100) \times (0,10)$ has a low absorption $\kappa = 10^{-4}$ while the rest has $\kappa = 0.1$. In Kobayaski's test case 1A there is no scattering, and the three planes containing the origin reflects the radiations: (O,x,z), (O,x,y), (O,y,z).
Unfortunately the present method cannot handle volumic radiating region. Consequently we have kept the geometry but only the 3 faces of C inside Ω radiate in all directions $\boldsymbol{\omega}$ with intensity $Q^0[\boldsymbol{\omega}\cdot\mathbf{n}]_-$, where $\mathbf{n}$ is the normal to the cube's face pointing inside the cube. The domain is $\Omega = D \backslash C$.

3.2 Results

To assert the precision of the method we consider first only one reflective plane, $\Gamma_R = (0,y,z)$. So, $R_\nu = 1$ on that plane and zero elsewhere and Q^0 is non zero only on the faces of the C. We also take $\kappa = 0.1$ everywhere.
First we verify that the convergence is monotone increasing if T^0 is small and monotone decreasing if T^0 is large (Figure 2). Note that the monotone increasing sequence converges faster.
Next, we compare the results with a computation on a domain $\bar{D} = (-60,60) \times (0,100) \times (0,60)$ which is D plus the symmetrized of D with respect to the plane $(0,y,z)$. This is because reflection on a plane is equivalent to extending the domain by symmetry with respect to that plane.
Figure 4 shows level surfaces of J computed on the symmetrized domain (but restricted to the original domain) and compared with the same level surfaces but computed with the RC. Surfaces with similar colors should be near each other. In fact the difference is not viible except near $z = 0$.
Figure 5 shows level surfaces of J computed with the RC, $\kappa = 10^{-4}$ or 0.1, and the same level surfaces but computed without any RC on the (O,y,z) plane. It is seen that surfaces with similar color are far from each others. By comparing Figure 4 with Figure 5 we see that the RC does almost the same as symmetry and that no condition at all is a non viable approximation for this problem.

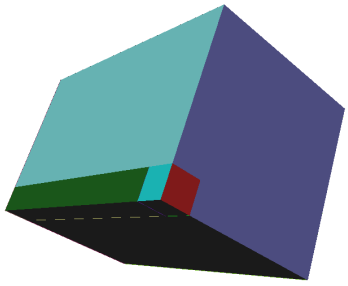

Figure 3: A small cube (colored blue and red on the figure) radiates normally to its faces in a medium which has a very small absorption coefficient $\kappa = 10^{-4}$ in the cylinder prolonging the cube and $\kappa = 0.1$ elsewhere.

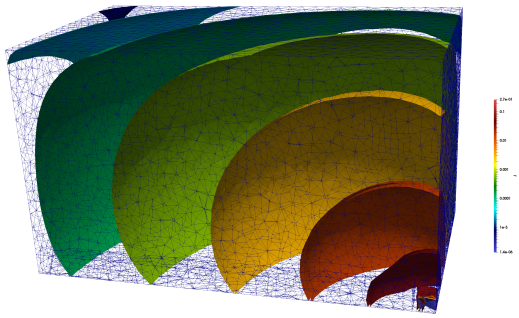

Figure 4: Level surfaces of J using a log scale computed with $\kappa = 0.1$ and only one reflective plane, $(0, y, z)$ facing us, slightly to the left. Comparison between a computation done with the RC and a computation done on a symmetrized domain, double in size.Surfaces of equal colors are so near each other that it is hard to distinguish them.

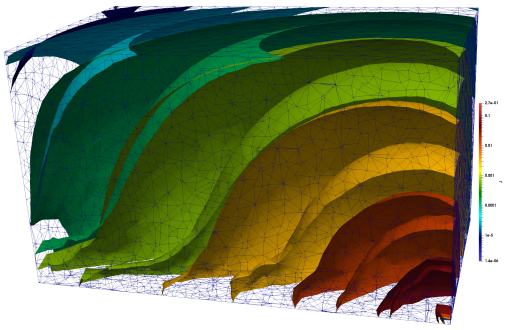

Figure 5: Same as in Figure 4 but the RC is not used in one computation. Surfaces of equal colors are far from those using the RC, indicating the absolute necessity of a RC.Here κ is not constant.

Similarly, figure 6 shows $x \mapsto J(x, 15, 15)$, computed on the symmetrized domain, or with the radiative condition or without it.

Finally, Figure 7 shows $x \mapsto J(x, 15, 15)$, computed with the RC on 3 meshes, coarse, medium and fine. The same 3 meshes are used in Table 1 where the theoretical complexity $N\sqrt[3]{N}\ln N$ is approximately observed. The compressing ratio for the surface and the volume matrices are shown too.

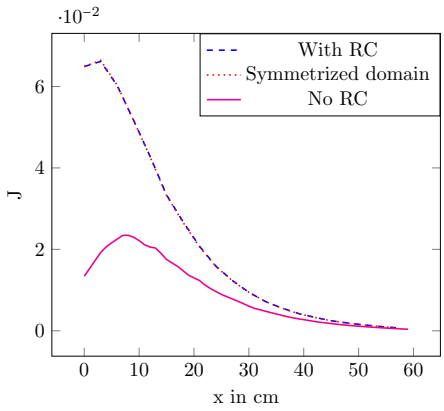

Figure 6: Values of J along the x axis at $y = z = 15$ computed by different methods on the coarse mesh.

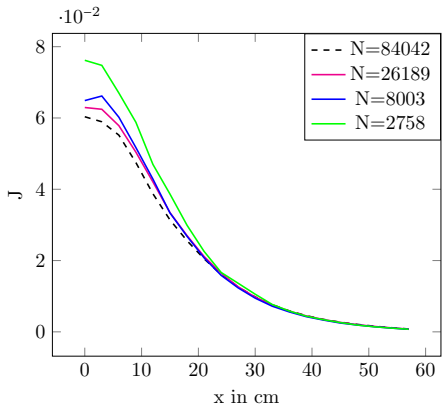

Figure 7: Values of J along the x axis at $y = z = 25$ computed with a RC with different meshes.

Table 1: CPU time, complexity and compression for 3 meshes with one reflective plane and non constant κ.

N vertices	Surf. Space Saving	Vol. Space Saving.	CPU	$\frac{10^5 CPU}{N\sqrt[3]{N}\log N}$
2758	0.41	0.60	5.2”	1.6971
8003	0.59	0.77	13.9”	0.97
26189	0.67	0.89	60.7”	0.77
84042	0.95	0.74	312”	0.75

But since the radiative sources are different (volumic in Kobayashi's and surfacic in our case) we have scaled the result with Kobayashi's value at $x = 5, y = 15, z = 5$ by their values at $y = 15$.

3.3 Kobayashi's Test 1A

Test 1A of [11] has been computed, i.e. non constant κ and 3 reflective planes. Surface levels of J are shown on Figure 10.
The comparison with the data in [11] on the line $(5, y, 5)$ is shown on Figure 8. Finally the L^2 error is computed using values on the line $(x, 15, 15)$. The reference solution to compute the error is the solution on a mesh with N=26189 .

The results are displayed on Figure 9. It shows an L^2-error on the line $O(h^3)$.

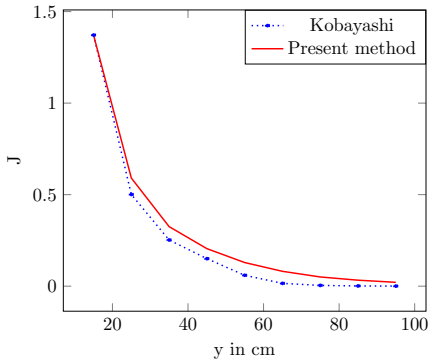

Figure 8: Values of J versus $y \geq 15$ at $x = z = 5$ and comparison with the values given in [11]. A scaling is applied to each curve so that they coincide at $y = 15$ (because [11] is given for volumic source and the present method handles only surface sources).

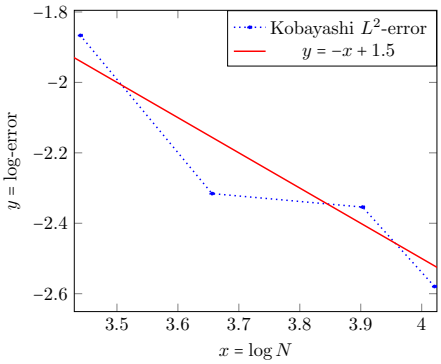

Figure 9: Log-log plot of L^2 error versus N. The line $-\log N + 1.5$ indicates an error $O(\frac{1}{N})$. The reference solution is computed on a mesh with 26189 vertices. The plotted points are computed on meshes with N as in Table 1.

Conclusion

Compressed H-matrices is an ideal tool for RTE in integral form because the complexity of the method is $O(N\sqrt[3]{N}\ln N)$ where N is the number of vertices in the 3D mesh and because it can handle frequency dependent absorption and scattering coefficients at the expense of a finite number of compressed matrices and a finite number of matrix-vector products.
The integral nonlinear formulation of RTE proposed in [5] has been extended to cases with reflective boundary conditions. The monotonicity property of the iterative solver is kept. The discretization with the finite element method is the same. However it is hard to write a general computer code because of the complexity of potential multiple reflections, as in Ray Tracing. Hence in this article the numerical validation has been done only for a finite number of plane reflective boundaries and for an academic geometry.

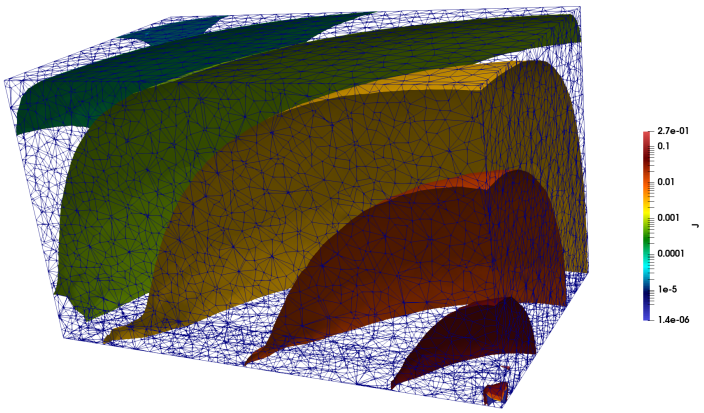

Figure 10: Kobayashi's test: Level surfaces of J using a log scale. The reflective planes are the $(O, x, z), (O, y, z), (O, x, y)$. The origin O is the lower right corner.

Acknowledgement

We would like to thank warmly Frédéric Hecht, for his constant good will to adapt `FreeFEM` to our needs.

References

[1] M. Bebendorf. Approximation of boundary element matrices. 86(4):565–589, 2000.

[2] M. Bebendorf. *Hierarchical Matrices*. Lecture notes in science and engineering. Springer, Heidelberg, 2008.

[3] S. Boerm, L. Grasedyck, and W. Hackbusch. Hybrid cross approximation of integral operators. *Numerische Mathematik*, 10(12):221–249, 2005.

[4] Yuwei Fan, Jing An, and Lexing Ying. Fast algorithms for integral formulations of steady-state radiative transfer equation. *J. Comp. Physics*, 380(1):191–211, 2019.

[5] F. Golse, F. Hecht, O. Pironneau, D. Smetz, and P.-H. Tournier. Radiative transfer for variable 3d atmospheres. *J. Comp. Physics*, 475(111864):1–19, 2023.

[6] F. Golse and O. Pironneau. Radiative transfer in a fluid. *RACSAM, Springer*, Volume dedicated to I. Diaz(doi.org/10.):https://doi.org/10.1007/s13398–022–01362–x, 2022.

[7] F. Golse and O. Pironneau. Stratified radiative transfer in a fluid and numerical applications to earth science. *SIAM Journal on Numerical Analysis*, 60(5):2963–3000, 2022.

[8] W. Hackbusch. A sparse matrix arithmetic based on h-matrices. part i: Introduction to h-matrices. *Computing*, 62(2):89–108, 1999.

[9] F. Hecht. New developments in freefem++. *J. Numer. Math.*, 20:251–265, 2012.

[10] P. Jolivet, M.A. Badri, and Y. Favennec. Deterministic radiative transfer equation solver on unstructured tetrahedral meshes: Efficient assembly and preconditioning. *Journal of Computational Physics*, 437:110313, 2021.

[11] K. Kobayashi, N. Sugimura, and Y. Nagaya. 3d radiation transport benchmark problems and results for simple geometries with void region. *Prog. Nucl. Energy*, 39:119–144, 2001.

[12] Dimitri Mihalas and Barbara Weibel Mihalas. *Foundations of radiation hydrodynamics*. New York, Oxford: Oxford University Press, 1984.

[13] G. Pomraning. *The equations of Radiation Hydrodynamics*. Pergamon Press, NY, 1973.

[14] S. Rjasanow and O. Steinbach. *The Fast Solution of Boundary Integral Equations*. Mathematical and Analytical Techniques with Applications to Engineering. Springer, Heidelberg, 2007.

[15] S. Sauter and C. Schwab. *Boundary Element Methods*, volume 39 of *Springer Series in Computational Mathematics*. Springer, Heidelberg, 2011.

[16] C. Siewert. On radiative-transfer problems with reflective boundary conditions and internal emission. *Journal of Applied Mathematics and Physics ZAMP*, 35:144–155, 1984.

[17] T. Tarvainen, M. Vauhkonen, V. Kolehmainen, and J. P. Kaipio. Hybrid radiative-transfer-diffusion model for optical tomography. *Applied optics*, 44(6):876–886, 2005.

Declarations

- As to the specific input of each author, P.-H. Tournier provided the $\mathcal{H}$-matrices part and the interface between `htool` and `FreeFEM`; the rest of the program and the theory were done together.
- The authors have no relevant financial or non-financial interests to disclose.
- The authors have no conflicts of interest to declare that are relevant to the content of this article.
- All authors certify that they have no affiliations with or involvement in any organization or entity with any financial interest or non-financial interest in the subject matter or materials discussed in this manuscript.
- The authors have no financial or proprietary interests in any material discussed in this article.